Supporting Information of

Model Evaluation of New Techniques for Maintaining High-NO Conditions in Oxidation Flow Reactors for the Study of OH-Initiated Atmospheric Chemistry

Zhe Peng,[†] Brett B. Palm,[†] Douglas A. Day,[†] Ranajit K. Talukdar,[†] Weiwei Hu,[†] Andrew T. Lambe,[‡,§] William H. Brune,[∥] and Jose L. Jimenez[*†]

[†] Cooperative Institute for Research in Environmental Sciences and Department of Chemistry, University of Colorado, Boulder, CO 80309, USA

[‡] Chemistry Department, Boston College, Chestnut Hill, MA 02467, USA

[§] Aerodyne Research, Inc., Billerica, MA 01821, USA

[∥] Department of Meteorology, Pennsylvania State University, University Park, PA 16802, USA

Corresponding Author:

[*] Jose L. Jimenez. Email: jose.jimenez@colorado.edu

(a) OFR185-cNO

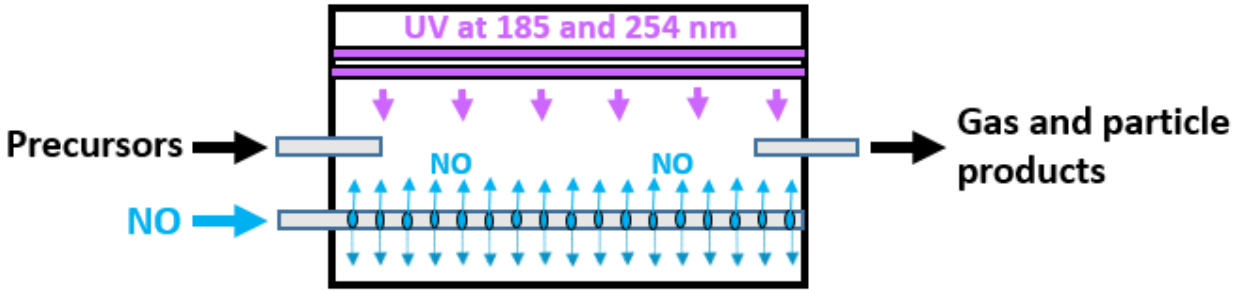

Main HO_x and NO production processes:

- $H_2O + h\nu(185\ nm) + O_2 \rightarrow \rightarrow OH + HO_2$
- $3O_2 + h\nu(185\ nm) \rightarrow \rightarrow 2O_3$
- $O_3 + h\nu(254\ nm) \rightarrow O(^1D) + O_2$
- $O(^1D) + H_2O \rightarrow 2OH$
- Continuous NO injection

16

(b) OFR254-iN_2O

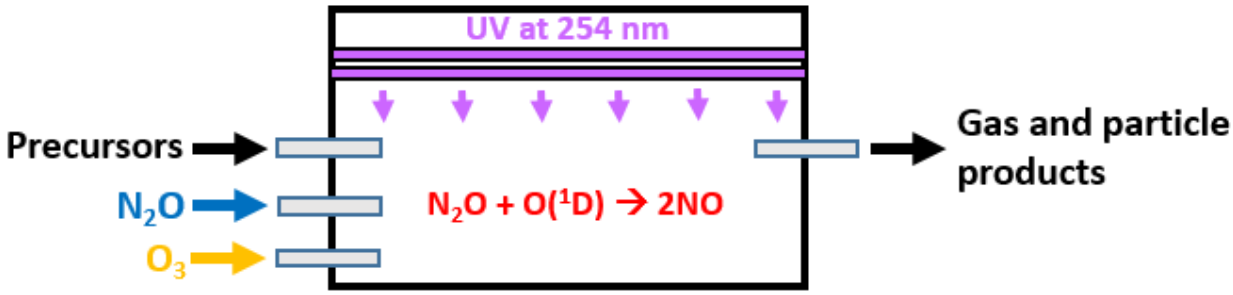

Main HO_x and NO production processes:

- $O_3 + h\nu(254\ nm) \rightarrow O(^1D) + O_2$
- $O(^1D) + H_2O \rightarrow 2OH$
- $N_2O + O(^1D) \rightarrow 2NO$

17

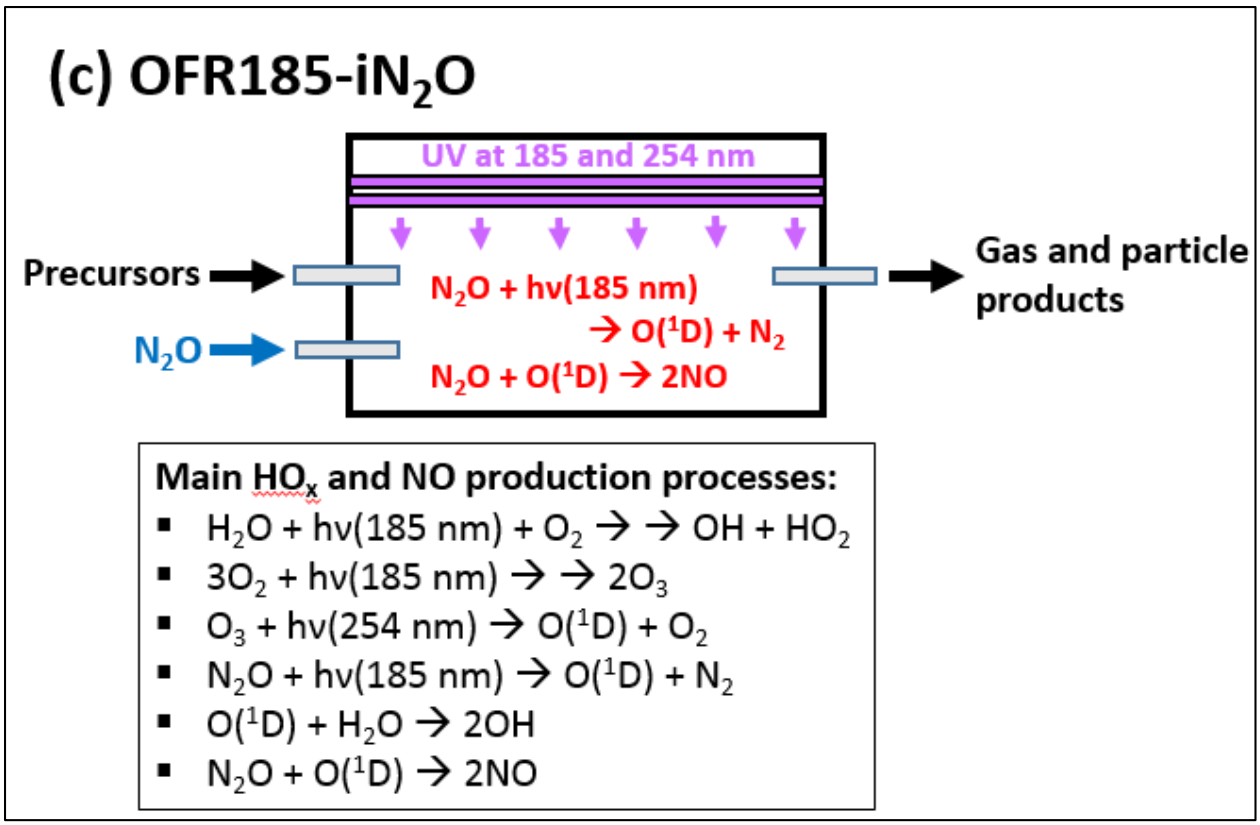

Figure S1. Schematics of the three new designs for maintaining high-NO evaluated in this study. Two consecutive arrows ("→ →") denotes that the corresponding reaction is not elementary and some elementary steps are omitted.

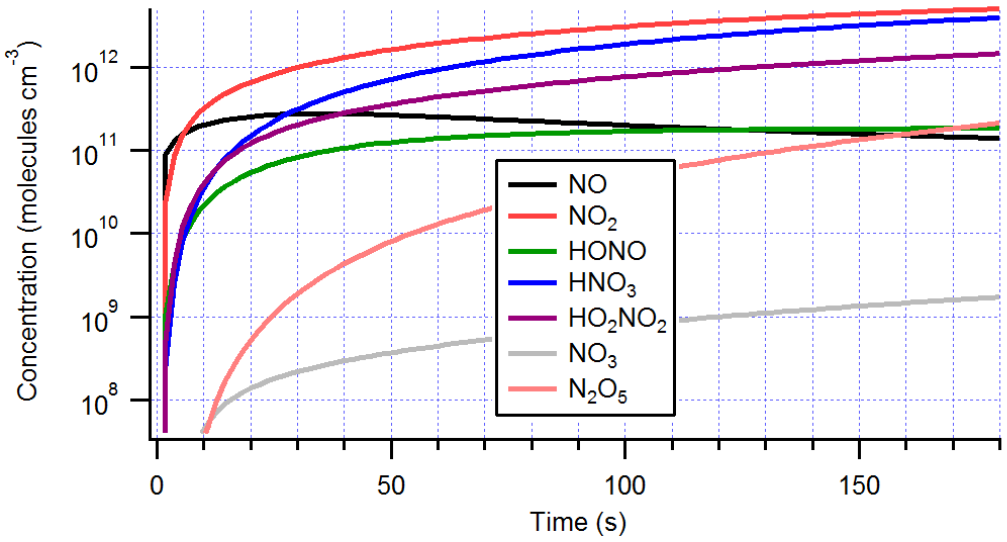

(a) OFR185-cNO

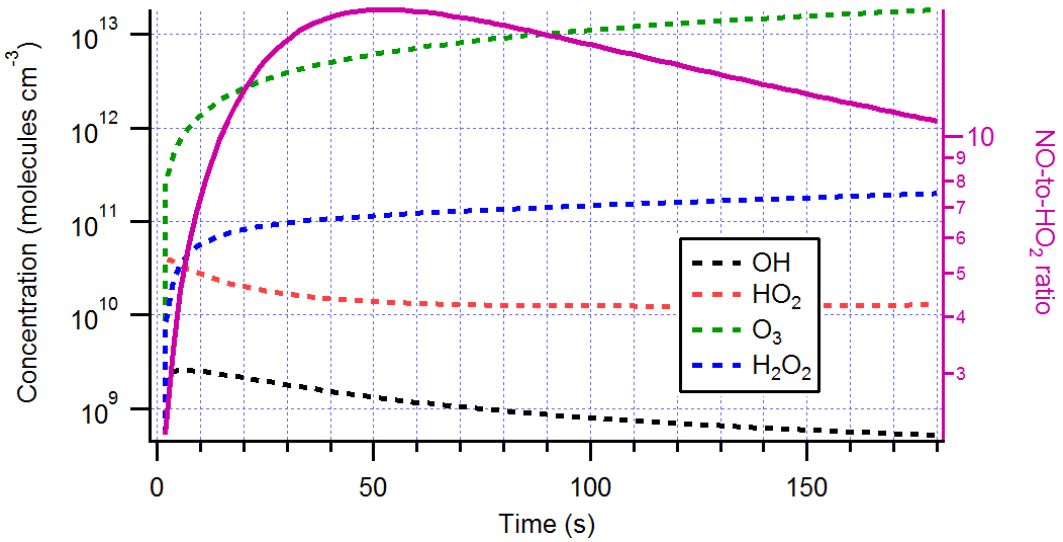

(b) OFR185-cNO

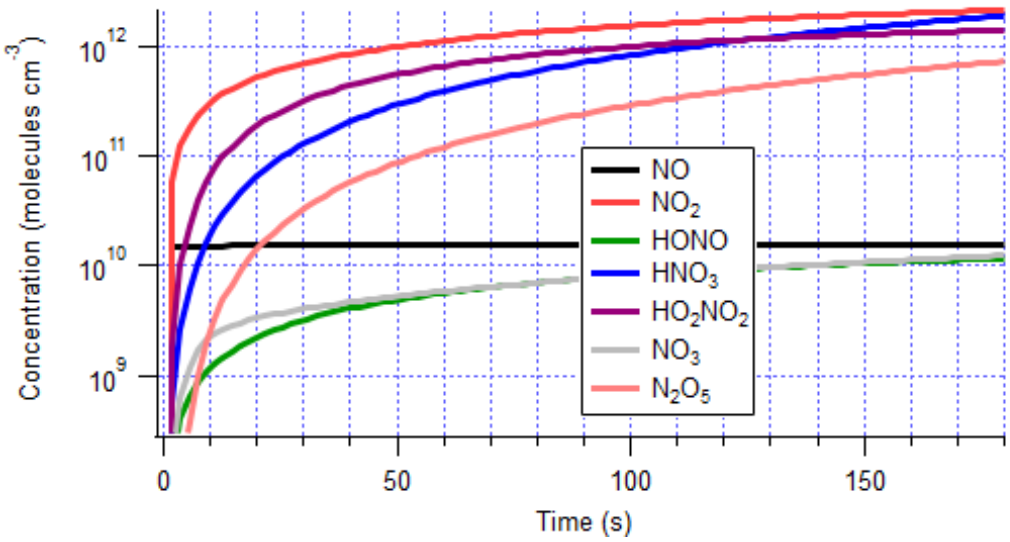

(c) OFR254-5-iN_2O

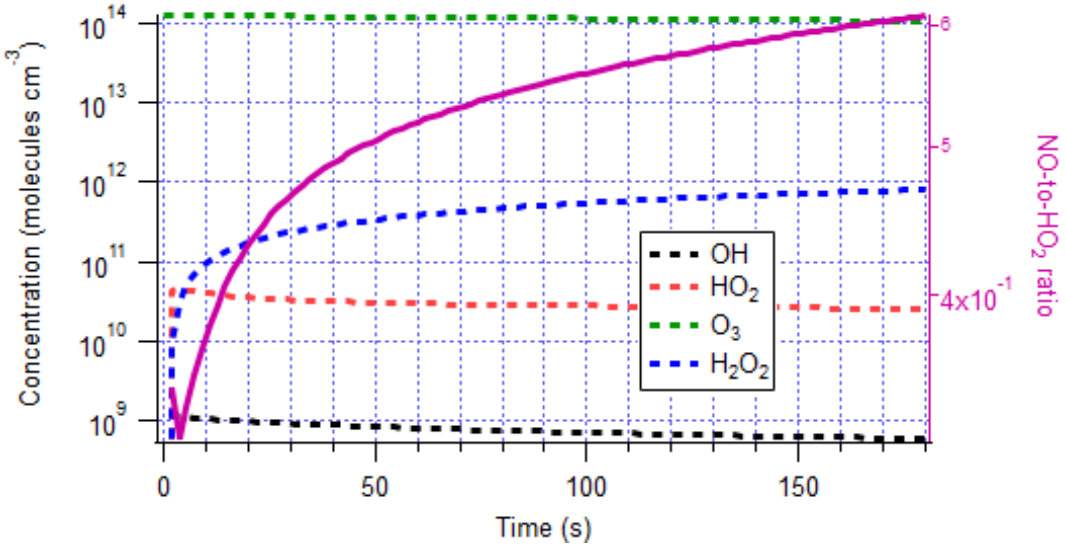

(d) OFR254-5-iN_2O

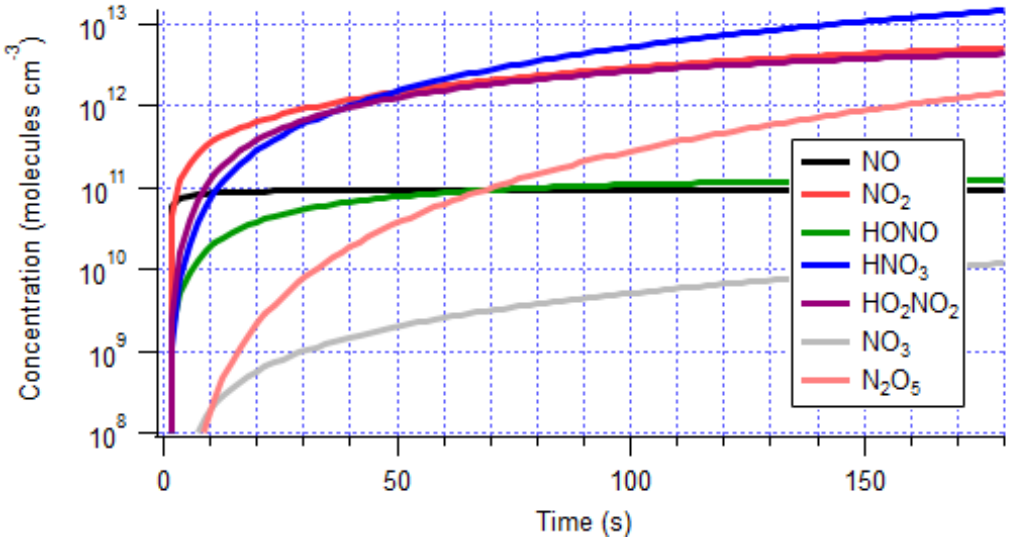

(e) OFR185-iN_2O

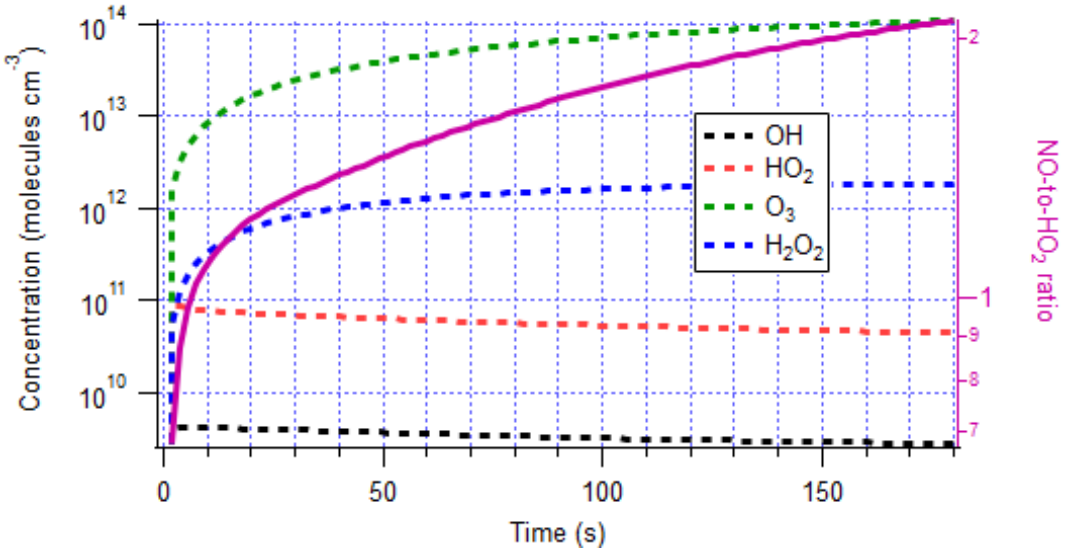

(f) OFR185-iN_2O

Figure S2. Concentrations of (a, c, e) several NO_y species and (b, d, f) OH, HO_2, O_3, and H_2O_2 and ratio of NO concentration to that of HO_2 as a function of reaction time in the cases shown in Fig. 1 (OFR185-cNO, OFR254-iN_2O, and OFR185-iN_2O).

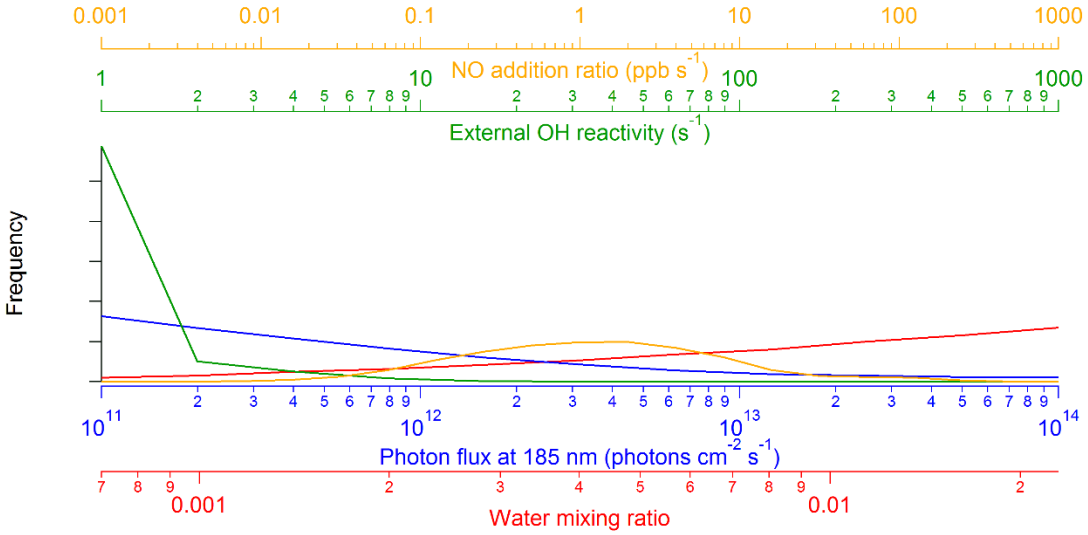

(a) OFR185-cNO

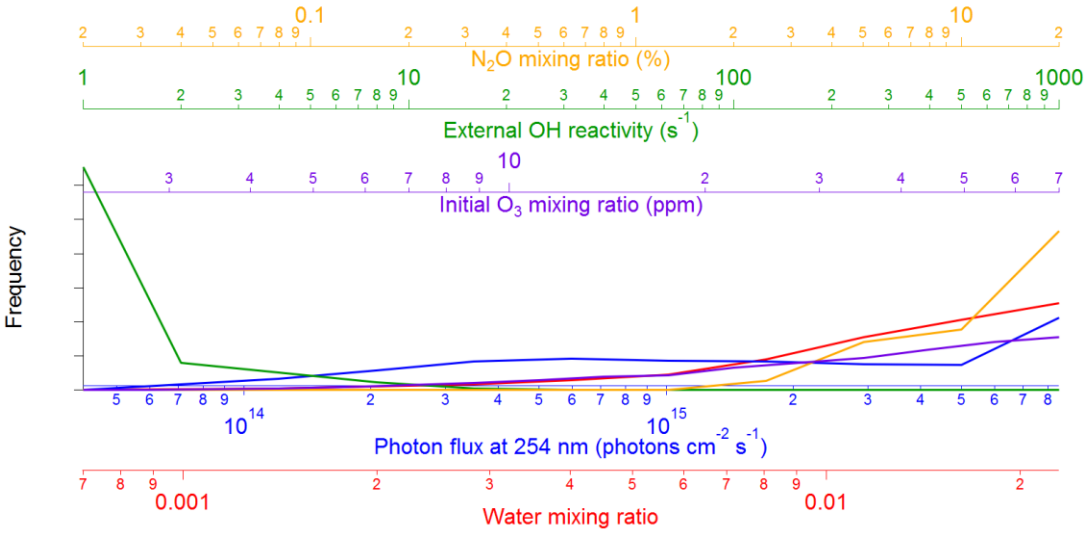

(b) OFR254-iN_2O

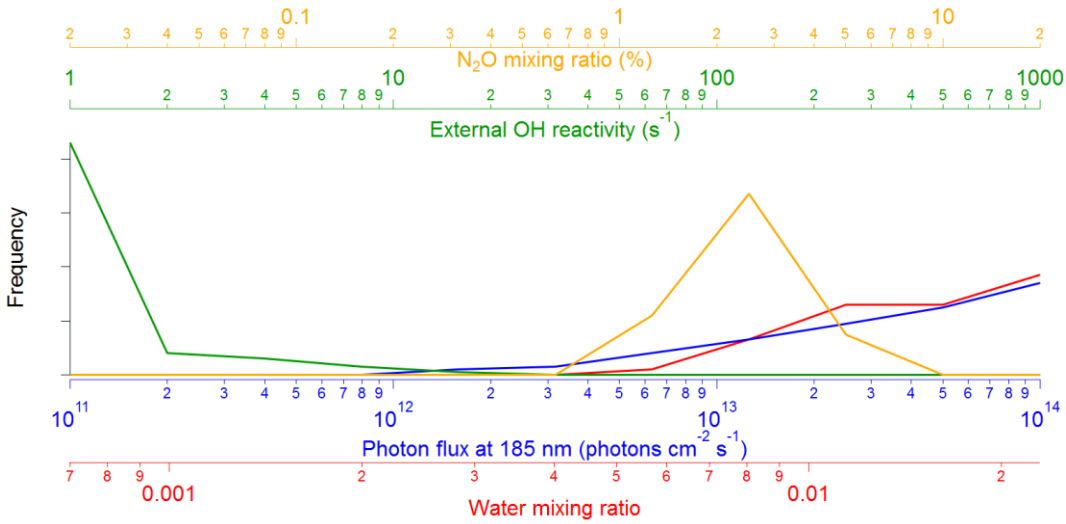

(c) OFR185-iN_2O

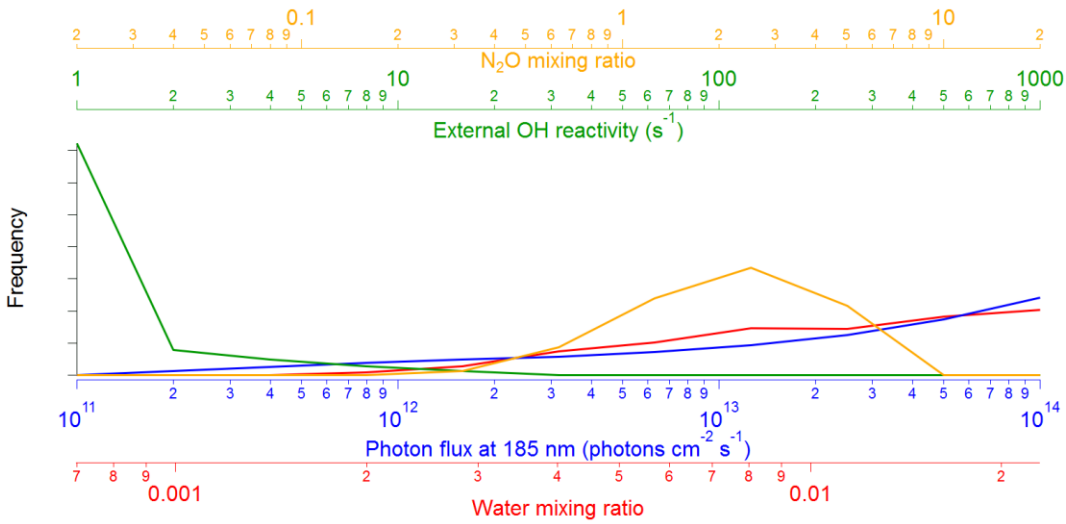

(d) OFR185-iN$_2$O (low O$_2$)

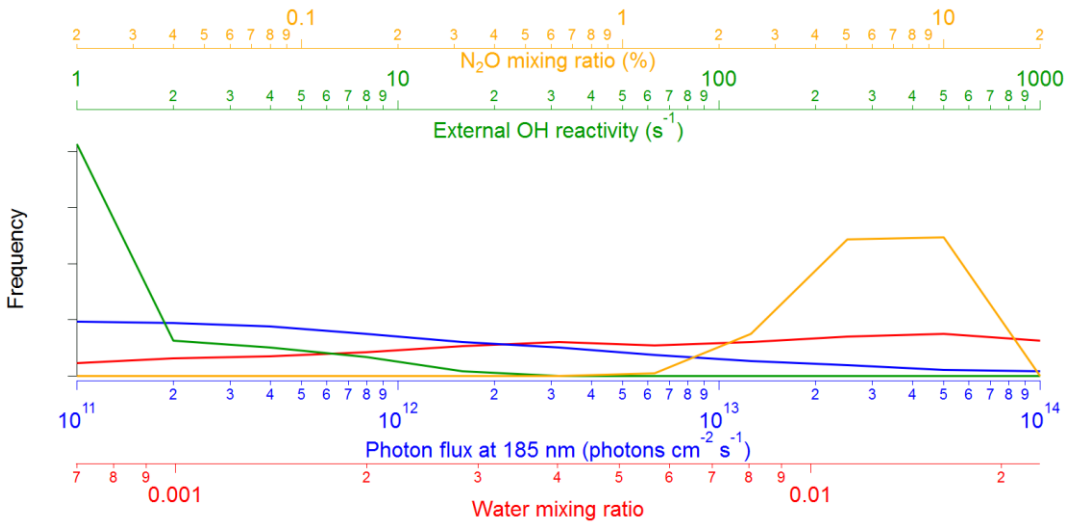

(e) OFR185-iN$_2$O (high F185/F254)

Figure S3. Frequency occurrence distributions of good high-NO conditions over physical inputs for (a) OFR185-cNO, (b) OFR254-iN$_2$O, (c) OFR185-iN$_2$O, (d) OFR185-iN$_2$O (with 0.2% O$_2$), and (e) OFR185-iN$_2$O (with an F185/F254 of 5%). See Table 2 for the definitions of the good high-NO conditions.

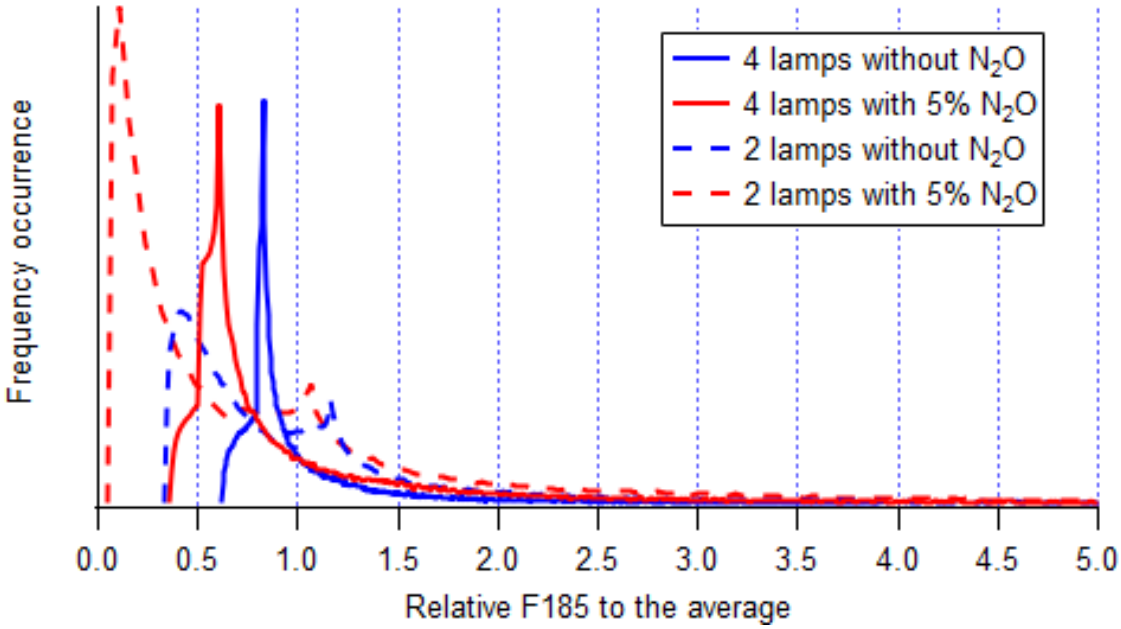

Figure S4. Probability distributions of relative photon flux at 185 nm to the average in OFR185 with 2 or 4 lamps and with or without 5% N_2O.

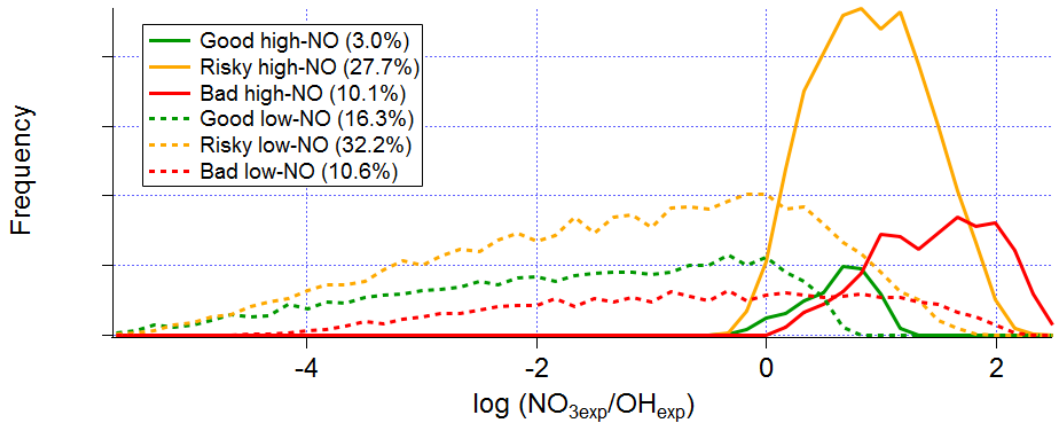

(a) OFR185-iN_2O (low O_2)

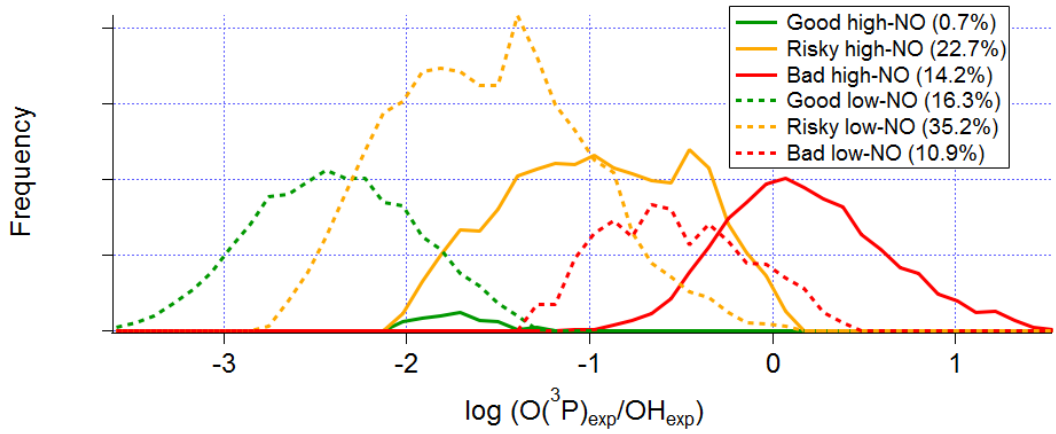

(b) OFR185-iN_2O

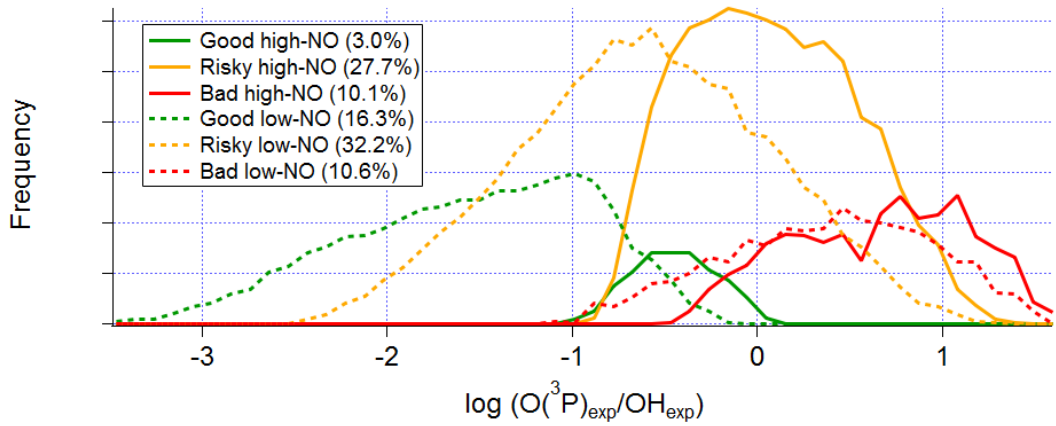

(c) OFR185-iN_2O (low O_2)

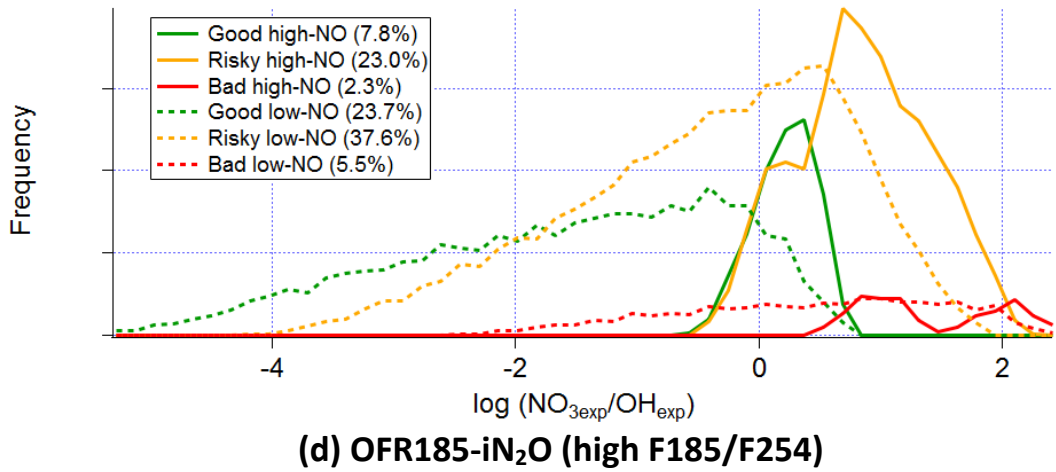

Figure S5. Frequency occurrence distributions of good/risky/bad (high/low-NO) conditions over logarithms of exposure ratios between NO_3 and OH for OFR185-iN_2O (a) with 0.2% O_2 and (d) with a F185/F254 of 5% and between $O(^3P)$ and OH for (b) OFR185-iN_2O and (c) OFR185-iN_2O with 0.2% O_2.

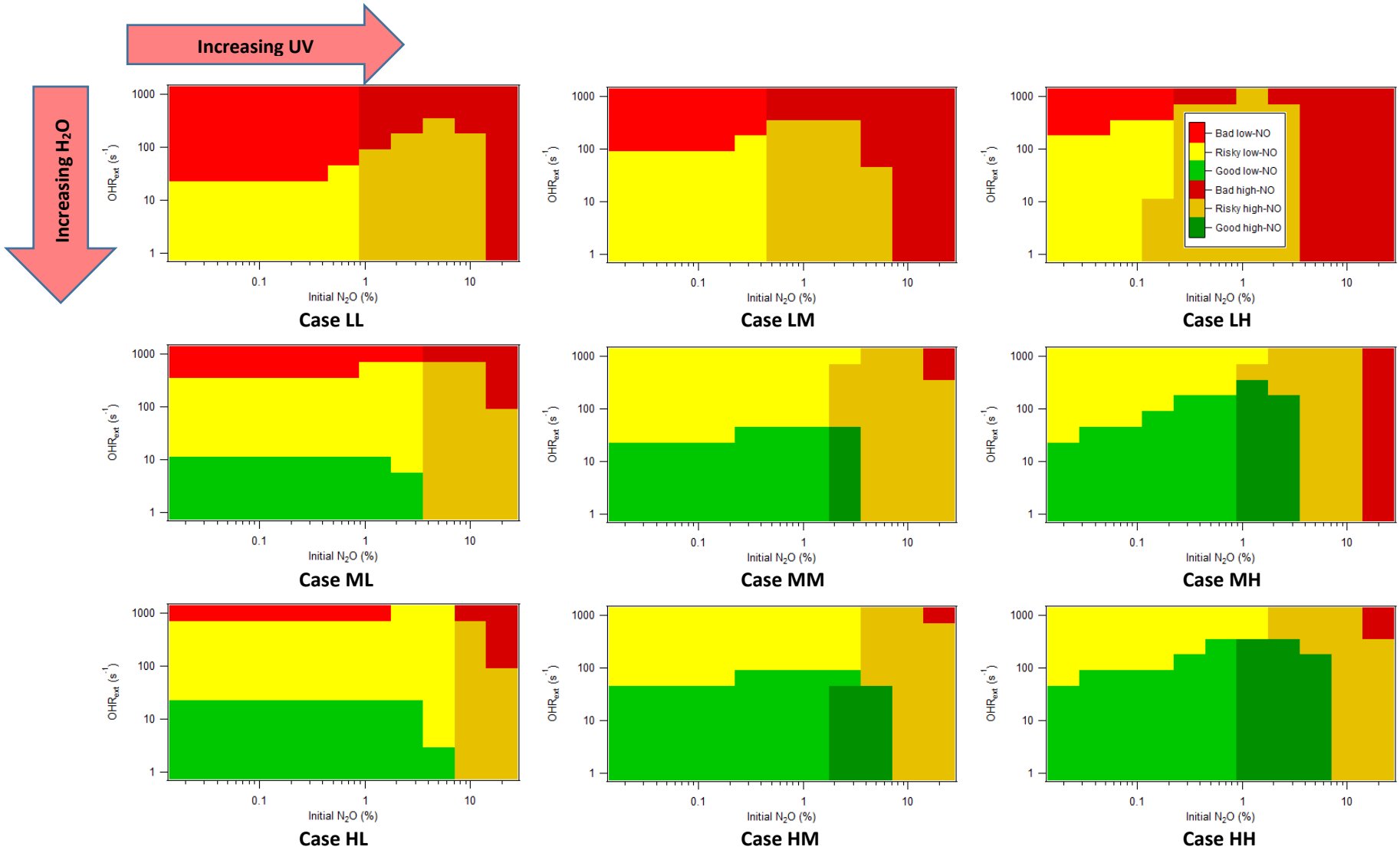

Figure S6. Same format as Fig. 4, but for OFR185-iN_2O with 0.2% O_2.

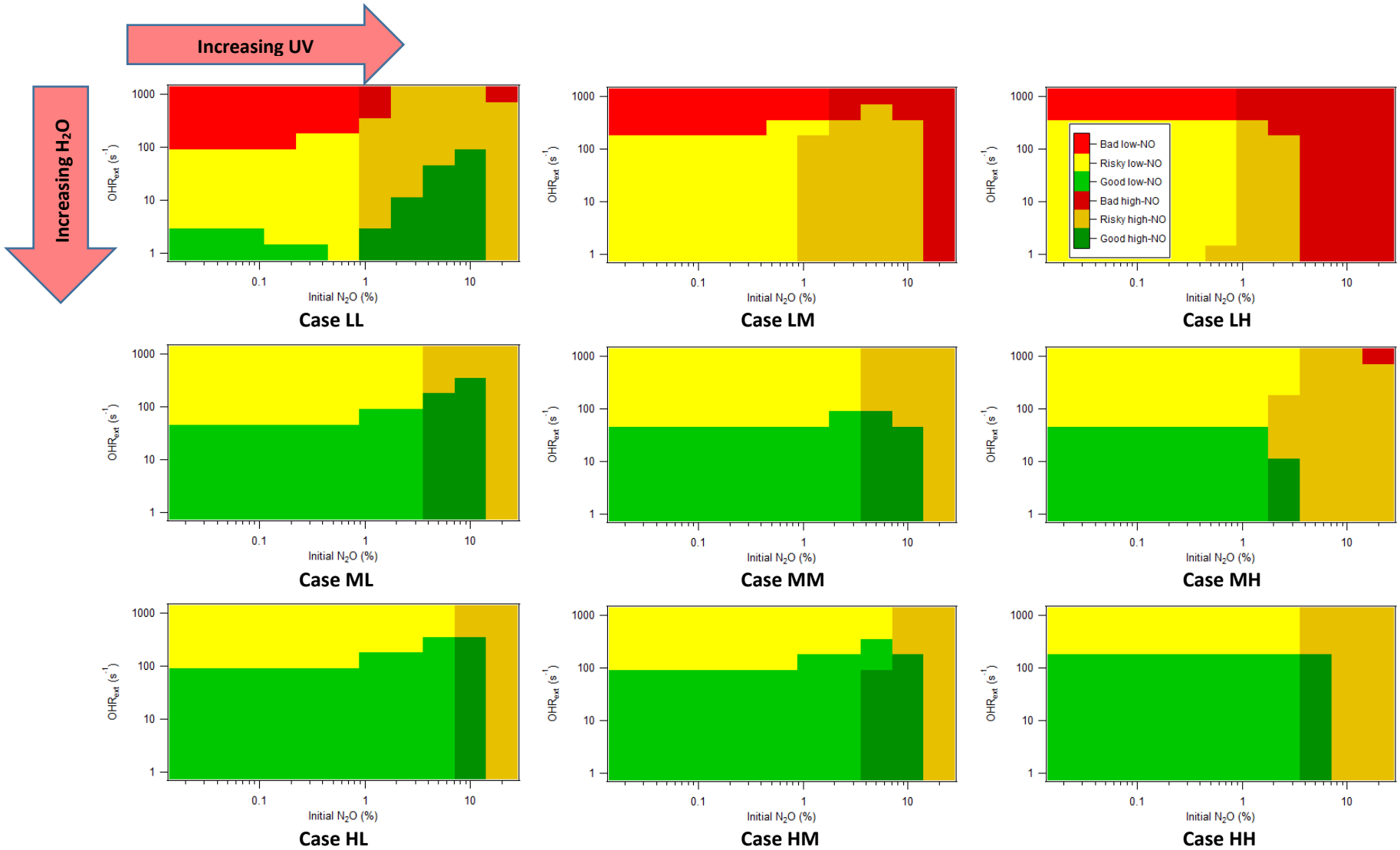

Figure S7. Same format as Fig. 4, but for OFR185-iN_2O with a F185/F254 of 5%.

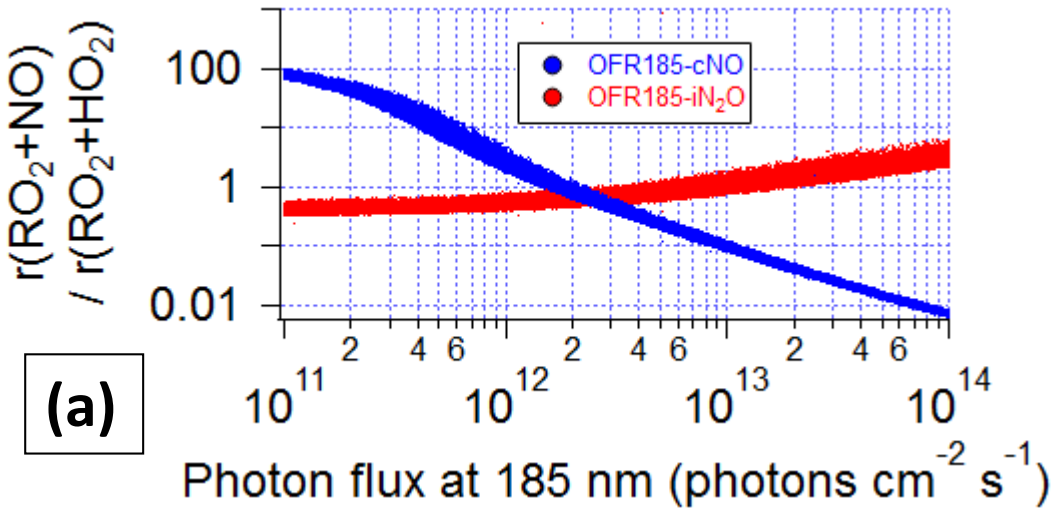

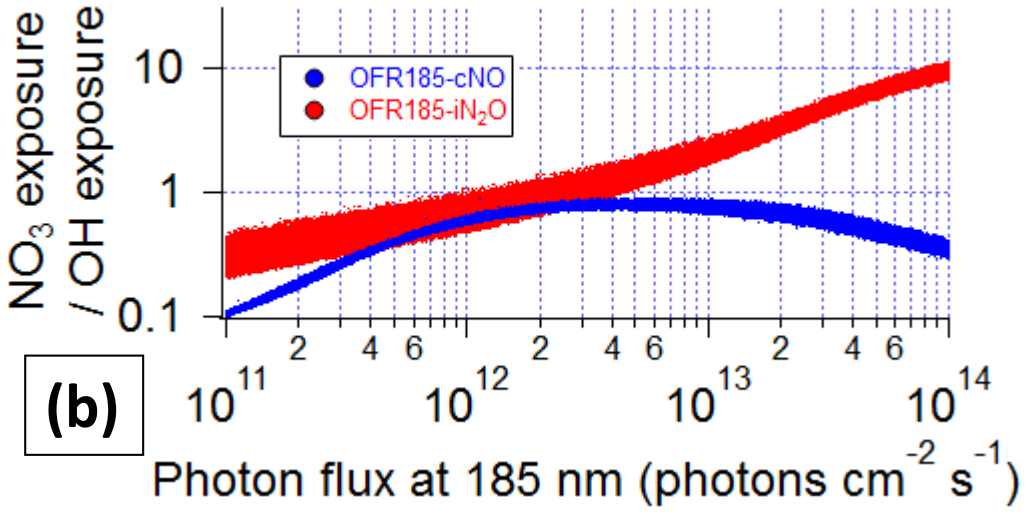

Figure S8. Scatter plots of (a) $r(RO_2+NO)/r(RO_2+HO_2)$ and (b) NO_{3exp}/OH_{exp} vs. F185 for the cases with ambient inputs of temperature, H_2O, and OHR_{ext} from SOAS field study, randomly selected UV, and rNO^{in}=2 ppb/s (for OFR185-cNO) or N_2O^{in}=3% (for OFR185-iN_2O). For more details of the inputs of these cases, see Section S1.

Table S1. Estimation equations of OH, NO_2, and NO_3 exposures and ratio of reactive flux of RO_2+NO to that of RO_2+HO_2 for OFR185-cNO, OFR185-iN_2O, and OFR254-iN_2O. UV in the equations for OFR185 and OFR254 are the photon fluxes at 185 and 254 nm, respectively. Exposures are in molecules cm^{-3} s, H_2O unitless, UV in photons cm^{-2} s^{-1}, OHR_{ext} in s^{-1}, $O_{3,in}$ in ppm, rNO^{in} in ppb s^{-1}, N_2O^{in} unitless, and residence time *t* in s. Number of fitted datapoints, average absolute value of the relative deviations (AAVRD) of the estimates by the equations from the fitted datapoints, and percentage of estimates out of a factor of 2 of modeled datapoints (Outlier percentage) are also shown.

Operation mode	Estimation equation	Number of fitted datapoints	AAVRD (%)	Outlier percentage
OFR185-cNO	$\log \mathrm{OH_{exp}} = 1.4925 + 0.84112 \log \mathrm{H_2O} + 0.93605 \log \mathrm{UV} - 0.40821 \log(0.053029 \cdot \mathrm{OHR_{ext}}) - 0.13011 \log \mathrm{rNO^{in}} - 0.12465(\log \mathrm{rNO^{in}})^2 + 0.13817 \log(0.053029 \cdot \mathrm{OHR_{ext}}) \cdot \log \mathrm{rNO_{in}} - 0.024808(\log \mathrm{rNO^{in}})^3 + \log(t/180)$	27951	41	19
	$\log(\mathrm{r(RO_2 + NO)/r(RO_2 + HO_2)}) = -7.0532 - 0.77641 \log \mathrm{H_2O} + 2.176 \log \mathrm{UV} - 0.2457 \log(0.053029 \cdot \mathrm{OHR_{ext}}) + 1.3428 \log \mathrm{rNO^{in}} + 0.16559(\log \mathrm{rNO^{in}})^2 + 0.029843(\log \mathrm{rNO^{in}})^3 - 0.14042(\log \mathrm{UV})^2$		55	29
	$\log \mathrm{NO_{2exp}} = -12.836 + 1.8654 \log \mathrm{H_2O} + 4.6604 \log \mathrm{UV} - 0.16471 \log \mathrm{H_2O} \cdot \log \mathrm{UV} - 1.8623 \log \mathrm{rNO^{in}} + 0.22523 \log \mathrm{UV} \cdot \log \mathrm{rNO^{in}} - 0.068328(\log \mathrm{rNO^{in}})^2 - 0.20312(\log \mathrm{UV})^2 - 0.018197(\log \mathrm{rNO^{in}})^3 + \log(t/180)$		55	33
	$\log \mathrm{NO_{3exp}} = 0.53522 - 0.018119 \log \mathrm{H_2O} + 0.85631 \log \mathrm{UV} - 0.090146 \log(0.053029 \cdot \mathrm{OHR_{ext}}) - 2.7659 \log \mathrm{rNO^{in}} + 0.23337 \log \mathrm{rNO^{in}} \cdot \log \mathrm{UV} - 0.47692\lvert\log \mathrm{rNO^{in}}\rvert^{1.3339} + \log(t/180)$		68	41
OFR185-iN_2O	$\log \mathrm{OH_{exp}} = 4.5729 + 0.77767 \log \mathrm{H_2O} + 0.46802 \log \mathrm{UV} - 1.9026 \log(0.053029 \cdot \mathrm{OHR_{ext}}) - 1.6968 \log \mathrm{N_2O^{in}} - 0.18407 \log \mathrm{N_2O^{in}} \cdot \log \mathrm{UV} + 0.18535 \log \mathrm{N_2O^{in}} \cdot \log(0.053029 \cdot \mathrm{OHR_{ext}}) + 0.14406 \log \mathrm{UV} \cdot \log(0.053029 \cdot \mathrm{OHR_{ext}}) - 2.3556\lvert\log \mathrm{N_2O^{in}}\rvert^{1.2694} + \log(t/180)$	14641	38	15
	$\log(\mathrm{r(RO_2 + NO)/r(RO_2 + HO_2)}) = -3.3568 + 0.12188 \log \mathrm{UV} \cdot \lvert\log \mathrm{N_2O^{in}}\rvert^{0.38477} - \log \mathrm{H_2O} + 0.23345 \log \mathrm{UV} - 0.38953(\log \mathrm{N_2O^{in}})^2 + 1.6815 \log \mathrm{N_2O^{in}} - 0.089369(\log \mathrm{N_2O^{in}})^3 - 0.089447 \log(0.053029 \cdot \mathrm{OHR_{ext}})$		34	10
	$\log \mathrm{NO_{2exp}} = -4.0392 - 0.33444 \log \mathrm{H_2O} + 1.1288 \log \mathrm{UV} - 14.386\lvert\log \mathrm{N_2O^{in}}\rvert^{1.5} - 14.734 \log \mathrm{N_2O^{in}} + 3.55(\log \mathrm{N_2O^{in}})^2 + \log(t/180)$		33	11
	$\log \mathrm{NO_{3exp}} = -2.8709 - 0.3351(\log \mathrm{N_2O^{in}})^3 + 0.80081 \log \mathrm{UV} - 0.088975 \log(0.053029 \cdot \mathrm{OHR_{ext}}) - 0.084044 \log \mathrm{N_2O^{in}} - 2.8001(\log \mathrm{N_2O^{in}})^2 - 0.48384 \log \mathrm{N_2O^{in}} \cdot \log \mathrm{UV} - 2.0429 \log \mathrm{H_2O} + 0.17734 \log \mathrm{H_2O} \cdot \log \mathrm{UV} + 0.14604 \log \mathrm{N_2O^{in}} \cdot \log \mathrm{H_2O} + \log(t/180)$		35	12

OFR254-iN_2O	$\log OH_{exp} = 4.8743 + 0.83757 \log H_2O + 0.41214 \log UV - 0.082962 \log(0.053029 \cdot OHR_{ext}) + 3.8224 \log O_{3,in} + 1.6179 \log N_2O^{in} - 0.23589\left((2.5 \cdot N_2O^{in})\right)^2 - 0.17025(\log(0.053029 \cdot OHR_{ext}))^2 + 0.12603 \log(2.5 \cdot N_2O^{in}) \cdot \log(0.053029 \cdot OHR_{ext}) - 0.19932 \log(2.5 \cdot N_2O^{in}) \cdot \log UV - 0.21057 \log UV \cdot \log O_{3,in} + \log(t/180)$	234256	31	9
	$\log(r(RO_2 + NO)/r(RO_2 + HO_2)) = -2.5169 - 1.0663 \log H_2O - 0.7398 \log UV + 0.060477(\log UV)^2 - 0.32204 \log O_{3,in} - 1.3207 \log(2.5 \cdot N_2O^{in}) + 0.033(\log(2.5 \cdot N_2O^{in}))^2 - 0.016813(\log(2.5 \cdot N_2O^{in}))^3 + 0.046499 \log(2.5 \cdot N_2O^{in}) \cdot \log(0.053029 \cdot OHR_{ext}) + 0.16192 \log(2.5 \cdot N_2O^{in}) \cdot \log UV - 0.22746 \log(2.5 \cdot N_2O^{in}) \cdot \log H_2O$		23	5
	$\log NO_{2exp} = 12.005 + 2.944 \log H_2O + 0.17631 \log UV - 0.21949 \log UV \cdot \log H_2O + 0.51464 \log O_{3,in} + 0.89696 \log(2.5 \cdot N_2O^{in}) - 0.0229(\log(2.5 \cdot N_2O^{in}))^2 + \log(t/180)$		28	7
	$\log NO_{3exp} = 0.27517 - 3.3766 \log H_2O + 0.71155 \log UV + 0.21731 \log UV \cdot \log H_2O + 1.1035 \log O_{3,in} - 29.058 \log(250 \cdot N_2O^{in}) - 0.25958(\log(250 \cdot N_2O^{in}))^2 - 0.1581 \log(250 \cdot N_2O^{in}) \cdot (\log UV)^2 - 0.0049287 \log(0.053029 \cdot OHR_{ext}) \cdot \log UV + 4.3563 \log(250 \cdot N_2O^{in}) \cdot \log UV + 0.13338 \log(250 \cdot N_2O^{in}) \cdot \log H_2O + \log(t/180)$		27	7

S1. Physical conditions of the cases with ambient inputs from field studies

In CalNex-LA[1], BEACHON-RoMBAS[2], and SOAS[3] field studies, 2, 6, and 6 weeks of time series of OFR185-related experimental data were recorded. We use these data to investigate what conditions the OFR185-cNO and OFR185-iN_2O techniques would lead to in these ambient settings. Note that we do not copy the identical OFR inputs recorded in those campaigns, as the OFRs in those studies were all under low-NO conditions. The data of ambient temperature, OHR_{ext} (measured to be around 25 s^{-1} in CalNex-LA and estimated to be 15 and 20 s^{-1} in BEACHON-RoMBAS and SOAS, respectively), and H_2O (0.014 ± 0.006 (mean ± 2 standard deviation), 0.015±0.007, and 0.027±0.007 in CalNex-LA, BEACHON-RoMBAS, and SOAS, respectively) in those studies are used in the present work, while OFR UV data are replaced by random samples with a log-uniform distribution covering the explored range of 185 nm photon flux in this study. For OFR185-cNO and OFR185-iN_2O modes, an rNO^{in} of 2 ppb/s and an N_2O^{in} of 3% are employed, respectively, as these values seem to be optimal according to Fig. S2. Instead of a scan over exponentially incremental levels, as done for other model cases, we adopt random samples for UV to avoid any correlation between them and ambient input time series. However, as the random samples cover the same ranges of UV as other model cases, and roughly as for the lamp setting scan in field studies, the differences between the outputs of model cases without ambient inputs and those with some ambient inputs result from those ambient inputs and the optimal rNO^{in} and N_2O^{in} values.

References

(1) Ortega, A. M.; Hayes, P. L.; Peng, Z.; Palm, B. B.; Hu, W.; Day, D. A.; Li, R.; Cubison, M. J.; Brune, W. H.; Graus, M.; et al. Real-Time Measurements of Secondary Organic Aerosol Formation and Aging from Ambient Air in an Oxidation Flow Reactor in the Los Angeles Area. *Atmos. Chem. Phys.* **2016**, *16*, 7411–7433.

(2) Palm, B. B.; Campuzano-Jost, P.; Ortega, A. M.; Day, D. A.; Kaser, L.; Jud, W.; Karl, T.; Hansel, A.; Hunter, J. F.; Cross, E. S.; et al. In Situ Secondary Organic Aerosol Formation from Ambient Pine Forest Air Using an Oxidation Flow Reactor. *Atmos. Chem. Phys.* **2016**, *16*, 2943–2970.

(3) Hu, W.; Palm, B. B.; Day, D. A.; Campuzano-Jost, P.; Krechmer, J. E.; Peng, Z.; de Sá, S. S.; Martin, S. T.; Alexander, M. L.; Baumann, K.; et al. Volatility and Lifetime against OH Heterogeneous Reaction of Ambient Isoprene-Epoxydiols-Derived Secondary Organic Aerosol (IEPOX-SOA). *Atmos. Chem. Phys.* **2016**, *16*, 11563–11580.